Article

Not peer-reviewed version

Development of Photothermal Catalyst from Biomass Ash (Bagasse) for Hydrogen Production via Dry Reforming of Methane (DRM): An Experimental Study.

Thongchai Rohitatisha Srinophakun *, Ittichai Kanchanakul, Sanchai Kuboon, Wasawat Kraithong, Hiroaki Kaneko, Akira Yamaguchi, Masahiro Miyauchi

Posted Date: 2 May 2023

doi: 10.20944/preprints202305.0079.v1

Keywords: Hydrogen production; Photothermal catalysis; Dry reforming of methane; Biomass waste; Bagasse ash

Article

Development of Photothermal Catalyst from Biomass Ash (Bagasse) for Hydrogen Production via Dry Reforming of Methane (DRM): An Experimental Study

Ittichai Kanchanakul [1], Sanchai Kuboon [2], Hiroaki Kaneko [3], Wasawat Kraithong [4], Masahiro Miyauchi [5], Akira Yamaguchi [6] and Thongchai Rohitatisha Srinophakun [7,*]

[1] Ittichai Kanchanakul, Interdisciplinary of Sustainable Energy and Resource Engineering, Faculty of Engineering, Kasetsart University, Thailand
[2] Sanchai Kuboon, NANOTEC, National Science and Technology Development Agency (NSTDA), Thailand
[3] Wasawat Kraithong, NANOTEC, National Science and Technology Development Agency (NSTDA), Thailand
[4] Hiroaki Kaneko, Department of Materials Science and Engineering, Tokyo Institute of Technology, Japan
[5] Prof. Masahiro Miyauchi, Department of Materials Science and Engineering, Tokyo Institute of Technology, Japan
[6] Prof. Akira Yamaguchi, Department of Materials Science and Engineering, Tokyo Institute of Technology, Japan
[7] Prof. Thongchai Rohitatisha Srinophakun, Department of Chemical Engineering, Kasetsart University, Thailand
* Correspondence: fengtcs@gmail.com or thongchai.sr@ku.th; Tel.: +66-2942-8555 (ext. 1214)

Abstract: Conventional hydrogen production, as an alternative energy resource, has relied on fossil fuels to produce hydrogen, releasing CO_2 into the atmosphere. Hydrogen production via the dry forming of methane (DRM) process is a lucrative solution to utilize greenhouse gases, such as carbon dioxide and methane, by using them as raw materials in the DRM process. However, there are a few DRM processing issues, with one being the need to operate at a high temperature to gain high conversion of hydrogen, which is energy intensive. In this study, bagasse ash, which contains a high percentage of silicon dioxide, was designed and modified for catalytic support. Modification of silicon dioxide from bagasse ash was utilized as a waste material and the performance was explored of bagasse ash-derived catalysts interacting with light irradiation and reducing the amount of energy used in the DRM process. The results showed that the performance of 3%Ni/SiO_2 bagasse ash WI was higher than that of 3%Ni/SiO_2 commercial SiO_2 in terms of the hydrogen product yield, with hydrogen generation initiated in the reaction at 300 °C. Using the same synthesis method, the current results suggested that bagasse ash-derived catalysts had better performance than commercial SiO_2-derived catalysts when exposed to an Hg-Xe lamp. This indicated that silicon dioxide from bagasse ash as a catalyst support could help improve the hydrogen yield while lowering the temperature in the DRM reaction, resulting in less energy consumption in hydrogen production.

Keywords: hydrogen production; photothermal catalysis; dry reforming of methane; Biomass waste; bagasse ash

1. Introduction

Substitutional energy sources have drawn the public's attention in recent years due to the consequences of fossil fuel consumption. One of the alternative energy sources is hydrogen (H_2), an energy carrier that allows energy transport in a usable form from one place to another[1]. Clean hydrogen can be produced in several ways, such as through electrolysis. However, one of the lucrative approaches is the dry reforming of methane (DRM) process, which uses greenhouse gases as feedstock to produce synthesis gases (H_2 and CO). There are a few drawbacks to the DRM reaction. First, it needs more than 700°C to reach optimal efficiency and conversion [2]. This is energy intense.

 doi:10.20944/preprints202305.0079.v1

Second, the coking formation occurs at high temperatures. Several transition metals and noble metals, including Rh, Ni, Ir, Ru, Pt, and Co, are known to be active as DRM catalysts. The active metals are usually dispersed as small (nanoscale) particles supported on porous ceramic supports, such as Al_2O_3, and SiO_2 [3], through catalytic synthesis methods. However, Ni is the most suitable active metal due to its comparatively lower cost to upscale production to the industrial scale. Despite the economical price of Ni, Ni catalysts suffer inevitably from rapid deactivation caused by coke deposition, or active metal sintering or both [4] and it is less stable compared to the other noble catalysts. The rate of carbon deposition was reported to decrease with rising reaction temperature [5]. However, the increment in temperature is not a reasonable way to stop carbon deposition due to energy use concerns. Several researchers reported an improvement of the temperature reduction in thermal catalysts for the DRM reaction, such as Rh, Ni, Pd, Co, Ir, and Ce supported on Al_2O_3 and SiO_2 [6–9]; nonetheless, these require a trade off with the higher cost of noble metals. Recently, a unique way of designing catalysts using plasmonic nanoparticles (NPs) has appeared to be an attractive approach for the DRM reaction to reduce the operating temperature. The plasmonic/metal NPs interact with light incidents, such as sunlight or light sources with heat, by transferring photoexcited charge carriers from metal NPs to the reactants, leading to chemical transformations under less energy-intense conditions. In this case, it is ideally possible to target electronic excitation so that only DRM reactions are activated. This leads to the sustainability goals by lowering the operating temperature that traditionally runs at high temperatures and by improving the selectivity of reactions that may undergo side reactions.

Sugar is one of the top export products from Thailand. However, despite all the profits from the sugar industry, sugar production generates massive waste materials, such as bagasse, press mud, and spent wash[10]. Biomass waste from sugar production, like bagasse, could be used as fuel for thermal power plants or boiler stations to produce energy that can be fed back into sugar production. However, residuals ash from burning bagasse would be disposed of at landfills, which could bring about other environmental issues caused by the bagasse ash.

The current study focused on utilizing waste materials (bagasse ash) and modifying their properties as a catalyst support for photothermal catalyst in the DRM reaction compared with a commercial support catalyst (SiO_2). Furthermore, we used a conventional wet impregnation approach to obtain Ni/SiO_2 catalysts in a synthesis design strategy.

2. Results and Discussion

2.1. Fabrication of The Catalyst Support Preparation And Synthesis Catalyst

In this work, catalyst support was prepared by extracting SiO_2 from bagasse ash using an acidic extraction approach (3% HCl reagent grade), then modifying its properties by KOH activation at a ratio of 1:4 [11] to maximize the surface area of extracted SiO_2. For catalyst synthesis, Ni/SiO_2 was synthesized by conventional wet impregnation. There are two mechanisms of wet impregnation. One relies on capillary action to draw the solution into the pores. The other is that the solution transport changes from a capillary action process to a diffusion process in the wet impregnation method [12].

Preprints (www.preprints.org) | NOT PEER-REVIEWED | Posted: 2 May 2023 doi:10.20944/preprints202305.0079.v1

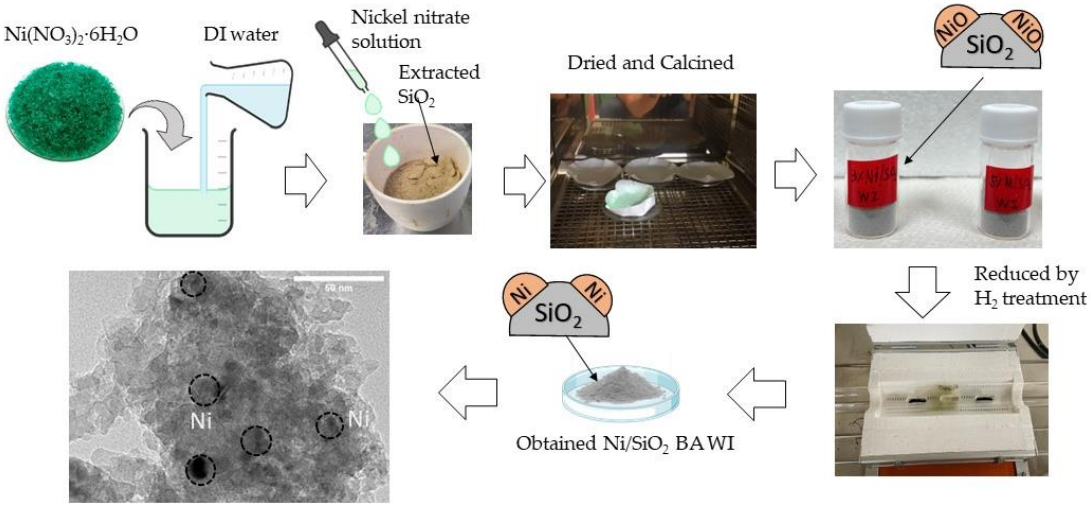

Figure 1. Schematic diagram of Ni/SiO_2 bagasse ash (BA) catalysts prepared using wet impregnation method (WI).

2.2. Characterization

The synthesized catalyst surface area was analyzed using an Autosorb® iQ3 gas sorption analyzer (Anton Paar QuantaTec Inc.; USA), in which adsorption-desorption isotherms take place with liquid nitrogen's help at -195 °C. The Brunauer-Emmett-Teller (BET) technique was used to calculate the catalyst surface area within the pressure range of 0.12 to 0.20. X-ray powder diffraction (XRD) patterns were recorded using a diffractor (XRD; Rigaku, Smartlab; Japan) axial diffractometer in the 2θ = 10° to 80° angular arrays with a step of 0.05°s^{-1} for the synthesized catalysts. Then, the synthesized catalysts were analyzed using X-ray fluorescence (Epsilon 1; Malvern Panalytical Ltd.; UK) for elemental analysis to confirm the chemical composition of the catalysts in percentage terms. Additionally, scanning electron microscopy (SEM) images of the synthesized catalysts were measured using Schottky field emission scanning electron microscopy (FE-SEM; SU8030; Hitachi-High Tech Corp.; Japan). The SEM images captured the surface morphology of the catalysts, and the EDS mapping checked the dispersion of Ni particles and the composition of the catalysts. Transmission electron microscopy (TEM) images were taken on a Jeol-JEM-2100Plus; Japan operated at 200 kV. Specimens were prepared by suspending sample powders in ethanol; then, and a drop of the suspension was deposited on copper grids.

2.2.1. XRD Analysis

As shown in **Figure 2**a, extracted SiO_2 was extracted by acidic extraction using HCl and followed by KOH activation at various ratios 1:2-1:6. These samples were characterized by X-ray diffraction analysis. The amorphous SiO_2 can be detected at 24.3°. The optimal ratio of KOH activation (SiO_2: KOH) was 1:4 [11]. Additionally, the XRD pattern of 3Ni/SiO_2 BA WI shows in **Figure 2**b, obtained by the Wet Impregnation approach. For a fresh 3Ni/SiO_2 catalyst (light green line), the diffraction peaks appearing at 37.1°, 43.1°, and 62.5° can be attributed to the NiO phase (JCPDS 65-2901), while the broad peak at 24.3° can be identified to the SiO_2 phase (JCPDS 39-1425)[13]. The XRD pattern of the reduced 3Ni/SiO_2 catalyst (blue line) also shows in Figure 1B which the diffraction peaks at 2θ = 44.3°, 51.4°, and 76.1°, which can be indicated by the crystal planes of (111), (200), and (220) of metallic nickel phase. Finally, the reduced 3Ni/SiO_2 WI catalyst after the DRM process (red line) shows that the XRD pattern demonstrated identically to the reduced 3Ni/SiO_2 WI catalyst (blue line) without the appearance of the diffraction peaks of carbon.

Preprints (www.preprints.org) | NOT PEER-REVIEWED | Posted: 2 May 2023 doi:10.20944/preprints202305.0079.v1

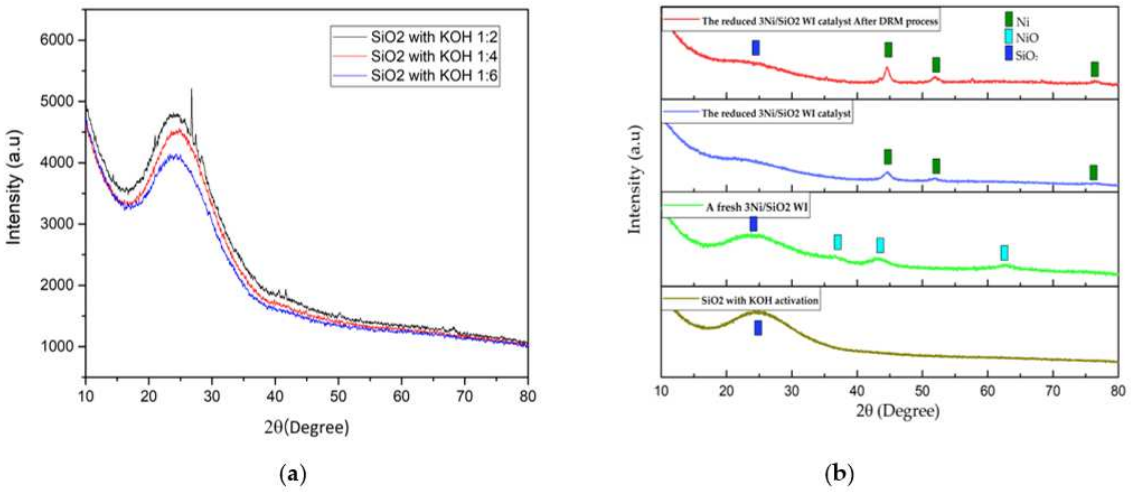

Figure 2. (**a**) The XRD pattern of extracted SiO_2 with KOH activation at various ratios of SiO_2 and KOH, (**b**) The XRD pattern of A fresh 3Ni/SiO_2 BA WI, the reduced 3Ni/SiO_2 WI and the reduced 3Ni/SiO_2 after the DRM process.

2.2.2. BET Surface Analysis

The BET analysis results are shown in Table 1. The BET surface area of the commercial SiO_2 was 10.7 m^2/g, which changed slightly to 11.4 and 12.6 m^2/g in the 3 and 5 Ni/SiO_2 commercial WI samples, respectively. The BET surface area of the extracted SiO_2 with KOH activation at a ratio 1:4 was 185 m^2/g, which marginally declined to 163 and 157 m^2/g in the 3 and 5 Ni/SiO_2 BA WI, respectively (**Table 1**). From the Barrett-Joyner-Halenda (BJH) method, the average pore sizes of the commercial SiO_2, the extracted SiO_2 with KOH activation, 3,5Ni/SiO_2 commercial WI, and 3,5Ni/SiO_2 BAWI were 4.47, 20.2, 4.62, and 20.9 nm, respectively.

Table 1. Physicochemical properties of extracted SiO_2 and Ni/SiO_2 WI catalyst.

Samples	BET[1] surface area (m^2/g)	Average pore size (nm)
Bare commercial SiO_2	10.7	4.47
Bare extracted SiO_2 from bagasse ash	42.3	36.0
Extracted SiO_2 BA, KOH activation 1:2	207	13.1
Extracted SiO_2 BA, KOH activation 1:4*	185	20.2
Extracted SiO_2 BA, KOH activation 1:6	178	11.6
3Ni/SiO_2 commercial WI	11.4	4.62
5Ni/SiO_2 commercial WI	12.6	4.85
3Ni/SiO_2 bagasse ash WI	163	20.9
5Ni/SiO_2 bagasse ash WI	157	20.9

[1] The Brunauer-Emmett-Teller (BET) technique.

2.2.3. SEM Analysis

As shown in **Figure 3**, the internal microstructures of the bare commercial SiO_2, extracted SiO_2 and the Ni/SiO_2 commercial WI were examined using SEM analysis, while EDS elemental mapping was used for the Ni/SiO_2 BA WI. The bare commercial SiO_2 is shown in **Figure 3**a, with a regular, smooth surface. **Figure 3**b shows an image of the extracted SiO_2 from BA with a complicated structure and a rough surface. **Figure 3**c,d represent synthesized Ni/SiO_2 commercial WI and Ni/SiO_2 BA WI, respectively. As seen, the Ni particles were successfully decorated on both the commercial SiO_2 and extracted SiO_2 BA surfaces. Furthermore, the extracted SiO_2 BA exhibited a complicated structure with a high surface area, which would be beneficial for photothermal catalytic activity. The EDS element spectra of the Ni/SiO_2 BA composite are shown in **Figure 3**e, which confirmed not only the

Preprints (www.preprints.org) | NOT PEER-REVIEWED | Posted: 2 May 2023 doi:10.20944/preprints202305.0079.v1

presence of Ni, Si, and O but also residual inorganic elements, such as Mg, Al, Fe, and K, on the synthesized catalyst. **Figure 3**f demonstrates the dispersion of Ni particles onto the catalyst support (SiO_2).

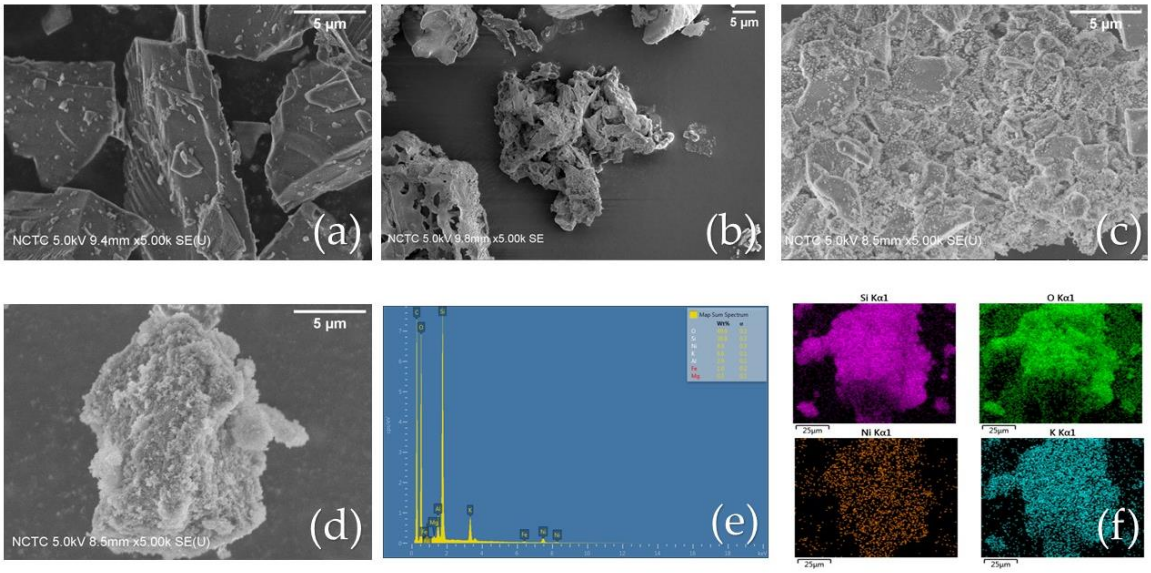

Figure 3. SEM images of (**a**) bare commercial SiO_2, (**b**) extracted SiO_2 from bagasse ash, (**c**) Ni/SiO_2 commercial WI, (**d**) Ni/SiO_2 BA WI. (**e**) EDS analysis of Ni/SiO_2 BA WI. (**f**) EDS mapping of Ni/SiO_2 BA WI.

2.2.4. XRF Analysis

Despite the EDS elemental mapping, XRF analysis helped to estimate the composition of the synthesized catalyst. The XRF analysis results indicated that Ni and SiO_2 were not only in the obtained samples, but there were also other residual elements, such as Al and K, as shown in **Table 2**. In contrast, the XRF analysis of Ni/SiO_2 commercial WI only exhibited Ni and Si as shown in **Table 3.**

Table 2. The elemental composition of Ni/SiO_2 BA WI.

Compounds	Concentration
Si	71.4 %
Ni	11.7 %
Al	5.26 %
K	11.7 %

Table 3. The elemental composition of Ni/SiO2 commercial WI.

Compounds	Concentration
Si	95.4 %
Ni	4.62 %

2.2.5. Optical Properties

The optical properties of the synthesized photothermal catalysts were evaluated using ultraviolet-visible spectroscopy. The UV-Visible diffuse reflectance spectrum (UV-Vis DRS) of bare SiO_2 commercial, extracted SiO_2 BA, 3,5Ni/SiO_2 commercial WI, and 3,5Ni/SiO_2 BA WI are shown in **Figure 4**a,b. The UV-Vis DRS of the commercial SiO_2 had a non-absorption edge at all wavelengths (blue DRS line in **Figure 4**a). In contrast, after the wet impregnation method, 3,5Ni/SiO_2 commercial WI exhibited an increment of absorption edge around 370 nm and strong absorption over a wide range of the UV and visible light regions (black and red DRS lines in **Figure 4**a). At the same time,

Preprints (www.preprints.org) | NOT PEER-REVIEWED | Posted: 2 May 2023 doi:10.20944/preprints202305.0079.v1

the UV-Vis DRS of the extracted SiO_2 from BA had an absorption edge around 230 nm (blue line in **Figure 4**b). It is because not only extracted SiO_2 from bagasse ash contain pure SiO_2, but it also consists of inorganic residuals such as Al, K, Mg, and Fe, which could add light adsorption properties to our extracted SiO_2 sample. Furthermore, after the wet impregnation method, 3,5Ni/SiO_2 BA WI demonstrated a similar trend to 3,5Ni/SiO_2 commercial WI, with an increment of strong absorption over a wide range of the UV and visible light regions (black and red DRS lines in **Figure 4**b).

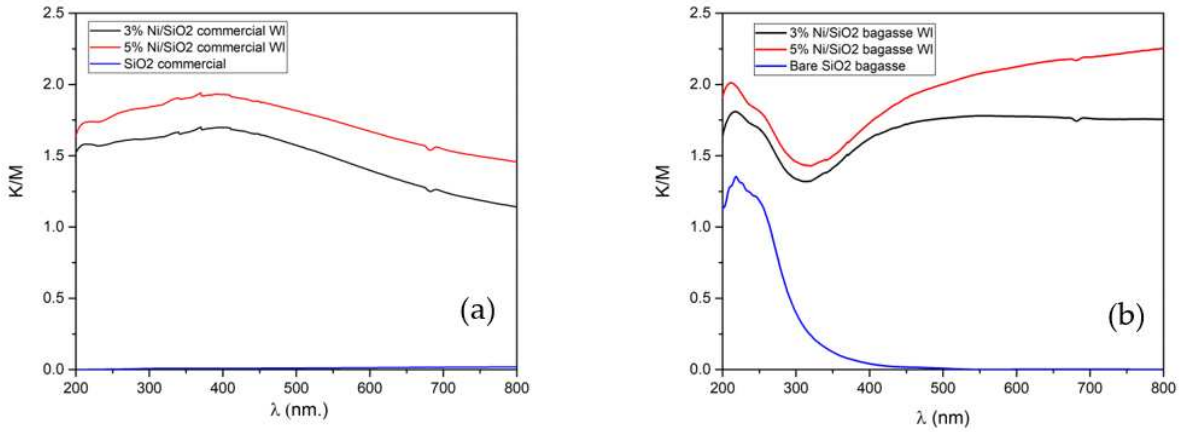

Figure 4. (**a**) UV-vis spectra of commercial SiO_2, 3,5Ni/SiO_2 comm WI, (**b**) UV-vis spectra of extracted SiO_2 from bagasse ash, 3,5Ni/SiO_2 BA WI.

2.3. Photothermal Catalytic Activity

2.3.1. Photothermal Catalytic hydrogen Generation Results and Analysis

The photothermal catalytic activities of the synthesized catalysts were examined based on CH_4, CO_2 conversion, and H_2 yield under UV-visible light irradiation. To investigate the efficient catalytic activity between different catalyst supports (commercial SiO_2 and extracted SiO_2 from bagasse ash), their catalytic performance toward H_2 generation was carried out under UV-visible light from an Hg-Xe lamp. The biomass-derived catalysts (Ni/SiO_2 BA WI) had higher activity than the commercial SiO_2 catalyst support one, as shown in **Figure 6**a,b because the surface area of Ni/SiO_2 BA WI was substantially higher than for the Ni/SiO_2 commercial WI, which could be attributed to higher activity. In addition, the light-adsorption ability of the extracted SiO_2 BA was enhanced after the wet impregnation method (**Figure 4**b) compared to the commercial SiO_2 before the wet impregnation method, which reflected light in all ranges. Therefore, it could interact with UV-visible light after the wet impregnation method (**Figure 4**a). **Figure 5** shows the relative intensity of the Hg-Xe lamp, which was intense in 200-450 nm range.

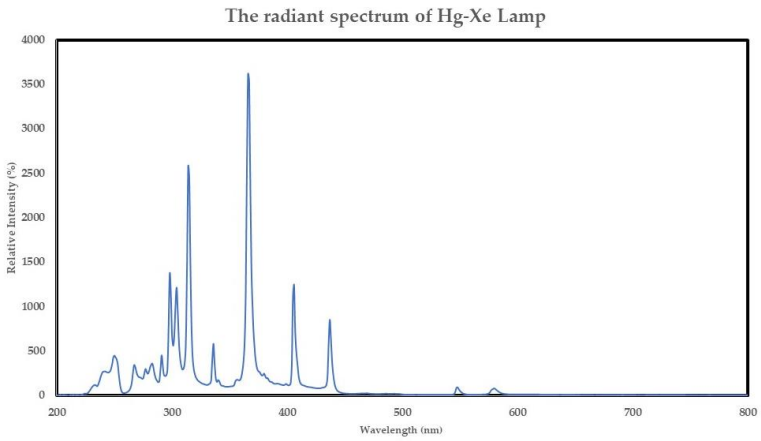

Figure 5. The radiant spectrum of Hg- Xe lamp.

Preprints (www.preprints.org) | NOT PEER-REVIEWED | Posted: 2 May 2023 doi:10.20944/preprints202305.0079.v1

2.3.2. Band alignment and proposed photothermal catalytic mechanism

Amorphous silica has a wide band gap energy of approximately 7.62–9.70 eV [14]; thus, the valence band electrons are relatively difficult to excite to the conduction band even when irradiated by UV light. However, the interband excitation in Ni particles was more favorable, with the photogenerated hot electrons overcoming the energy barrier. The hot carriers generated from the light-induced d-to-s interband excitation in Ni nanoparticles are proposed to mediate the transformation of photon energy to chemical energy. The relaxation of hot carriers increased the surface temperature of the catalyst and, more importantly, the separated hot carriers were directly involved in the chemical reaction[15].

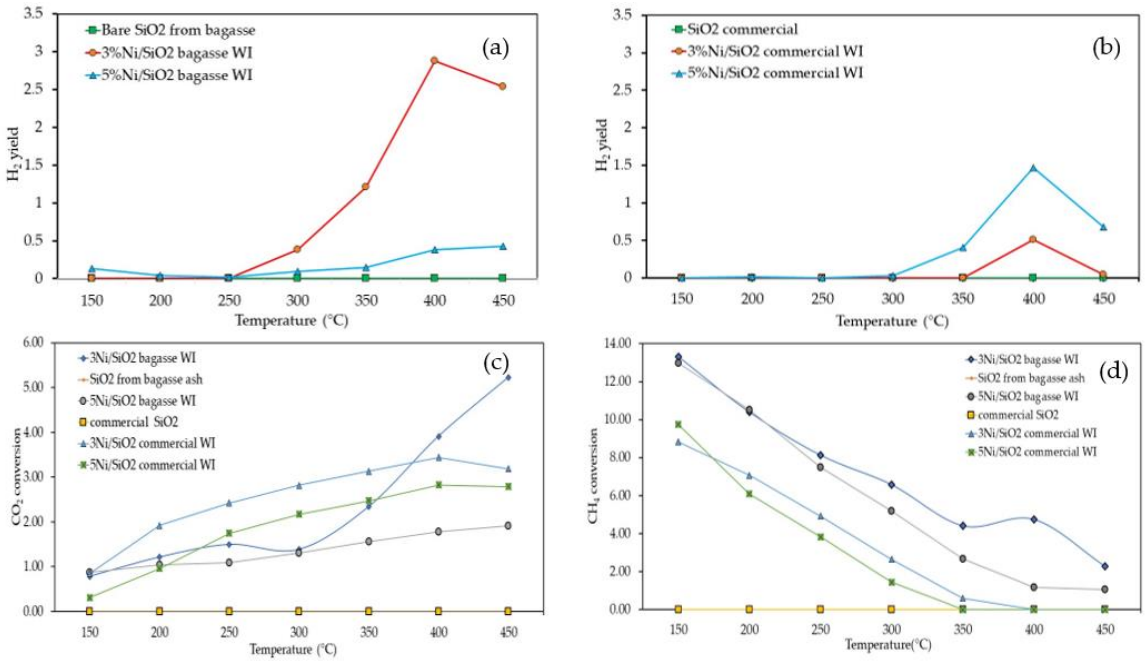

Figure 6. Photothermal catalytic activities of the synthesized catalysts (**a**) H_2 yield of Ni/SiO_2 from bagasse ash (**b**) H_2 yield of Ni/SiO_2 commercial (**c**) CO_2 conversion of synthesized catalysts (**d**) CH_4 conversion of synthesized catalysts.

To investigate the optimal Ni percentage amount on the synthesized catalysts with light irradiation, the photothermal catalytic performance of $3,5Ni/SiO_2$ BA WI and $3,5Ni/SiO_2$ commercial WI were tested in relation to the CH_4 and CO_2 conversions. **Figures 6**a,b revealed that $3Ni/SiO_2$ BA WI had the highest catalytic activity. However, when the content of Ni increased to 5%, the CO_2 conversion and H_2 yield were reduced, perhaps due to the agglomeration of nickel particles on the catalyst support. In addition, the light adsorption property of Ni/SiO_2 BA WI could have increased the surface temperature on the catalyst support, leading to sintering, which subsequently resulted in catalyst deactivation and reduced $5Ni/SiO_2$ BA WI performance.

In contrast, the CH_4 conversion of all synthesized catalysts showed a downward trend, indicating that the CH_4 reactant was consumed in the system, as shown in **Figure 6**d. An increase in the temperature resulted in reduced CH_4 conversion. Furthermore, H_2O appeared in the system.

The experimental results demonstrated that Ni particles on extracted SiO_2 from bagasse ash could interact with UV light to generate hydrogen at 300 °C because the UV-visible light provides photon energy to stimulate the Ni particles, leading to a plasmonic effect in the metal nanoparticles that creates electron-hole pairs (called hot carriers) and initiates the DRM reaction (eq. 1). However, when the temperature increased, the H_2 yield dropped at 450 °C and H_2O was detected in the system. Preferable reaction pathways, such as a reverse water gas shift reaction (eq. 2) at low temperatures (200–350 °C) may have resulted in a side reaction and unwanted products, such as H_2O in this case.

$$CH_4 + CO_2 \leftrightarrow 2H_2 + 2CO_2 \quad \Delta H°298k = +247 \text{ kJ mol}^{-1} \qquad (1)$$

 doi:10.20944/preprints202305.0079.v1

$$CO_2 + H_2 \leftrightarrow CO + H_2O \ \Delta H°298k = +41 \text{ kJ mol}^{-1} \quad (2)$$

3. Materials and Methods

3.1. Preparation of Bagasse Fly Ash

Bagasse fly ash was received from A Sugar Production Company (Thailand) after being burned as biomass fuel for the boiler. It contained a high moisture percentage; thus, it was necessary to dry the bagasse fly ash at 80 °C in a dry oven overnight followed by drying at 105 °C in an oven for 2 hours. After drying, the bagasse fly ash was fed into a crucible and burnt in a furnace at an initial temperature of 400 °C, a heating rate of 1 °C/min, and a holding time of 2 hours to de-volatized any organic compounds. Then, the ash was heated to 900 °C to de-carbonize it and held for 2 hours at the same heating rate to obtain crystalline silica.

3.2. Preparation of Silicon Dioxide Extraction

Bagasse fly ash was washed with 3% HCl reagent grade at a ratio of 12 ml 3% HCl per 1 g of bagasse fly ash as an extraction agent to reduce impurities other than SiO_2 in the bagasse fly ash. The washed ash was stirred using a magnetic stirrer at 240 rpm for 2 hours on a hotplate at 200 °C. After mixing, the sample was cleaned using deionized water until the pH was neutral. Afterward, the sample was passed through a vacuum filter containing filter papers and dried at 80 °C in a dry oven overnight. Then, the sample was calcined at 400 °C at a heating rate of 1 °C/min and cooled in the oven.

3.3. Preparation of KOH Activation For Silicon Dioxide

Silica dioxide is chemically activated by potassium hydroxide (KOH) at SiO_2-to-KOH ratios ranging from 1:1 to 1:8 to obtain SiO_2 particles with greater surface areas. The resulting mixed SiO_2 samples (~3 g) and KOH (1:1 to 1:8) were added to 100 mL of DI water and then stirred at 70 °C for 1 hour. After mixing, the samples were dried in the oven at 80 °C overnight until all the liquid had evaporated. Subsequently, each sample was placed in a ceramic crucible and calcined under an air atmosphere at 800 °C (heating rate 5 °C/min) for 1 hour. During the calcination process, porosity was induced in the silica structure by the combustion of K_2O derived from the KOH reaction. Next, the activated products were stirred with 2.5% HCl reagent grade to eliminate residual K_2SiO_3 in the samples. Afterward, the mixture was washed with DI water repeatedly to dissolve any KCl until the pH was neutral, followed by vacuum filtration to separate the solids from the liquid. Finally, the solid product was dried at 80 °C overnight to obtain the activated SiO_2 with a high surface area.

3.4. Preparation of Catalysts

Wet impregnation method

Nickel(II) nitrate hexahydrate ($Ni(NO_3)_2 \cdot 6\ H_2O$) is dissolved with DI water to obtain a Nickle nitrate solution. Then, a Nickle nitrate solution is dropped on the activated SiO_2 powder and mixed with a spatula. Subsequently, the samples are dried at 100 °C overnight and calcined at 600 °C for 2 hours to obtain a Ni/SiO_2 -WI.

3.5. Photothermal DRM activity test

The photothermal activities of the powder samples were measured under ambient pressure in a flow reactor with a quartz window[16], which enabled us to irradiate the powder samples with a 150 W Hg–Xe lamp (Hayashi-Repic, LA-410UV-5; Japan).. Approximately 10 mg of catalyst powder was put into a reactor; in sequence, the gas mixture CH_4: CO_2: Ar = 1: 1: 98 in vol% was continuously supplied to the reactor at a flow rate of 10 $mLmin^{-1}$. The generated hydrogen was measured using a micro gas chromatograph (Agilent, 3000 Micro GC; USA).

4. Conclusions

The Ni particles on extracted SiO_2 from bagasse ash (Ni/SiO_2 BA WI) and SiO_2, fabricated using acidic extraction and KOH activation, could drive the photothermal catalytic DRM reaction under UV light. Compared to Ni particles on commercial SiO_2 (Ni/SiO_2 commercial WI) with light irradiation, the Ni/SiO_2 BA WI could generate more H_2 products. In addition, light irradiation lowered the initiation temperature of syngas generation to 300 °C. However, the maximum H_2 yield was only 3%., As an assumption, the hot carriers generated from light-induced d to s interband excitation in the Ni particles played a vital role in our study, mediating the transformation of photon energy to chemical energy and driving the DRM reaction, despite the side reactions, such as the RWGS reaction. Therefore, we suggest that the use of extracted SiO_2 from bagasse ash as the catalyst support provides a perspective on substitute materials for a practical path to establish a plasmonic or non-plasmonic hot carrier-based photothermal catalytic system. The concept presented in this study showed the possibility of the utilization of waste materials as a solution for energy reduction in H_2 production. We expect that this concept will contribute to the progress of green energy and photothermal catalysis in the field of heterogeneous catalysis.

Author Contributions: Conceptualization, MM, SK, TRS, and IK; Investigation, IK, HK; methodology, IK and SK; Supervision, MM, TRS; Writing–original draft, IK; writing—review and editing, MM, TRS.

Funding: This research received funding through a TAIST-Tokyo Tech scholarship, National Science and Technology Development Agency (NSTDA), Thailand and the Faculty of Engineering, Kasetsart University, Bangkok, Thailand.

Conflicts of Interest: The authors declare no conflict of interest.

References

1. Remme, S.B.a.U., *The Future of Hydrogen.* IEA 2019. **Technology report**.
2. Arora, S. and R. Prasad, *An overview on dry reforming of methane: strategies to reduce carbonaceous deactivation of catalysts.* RSC Advances, 2016. **6**(110): p. 108668-108688.
3. Kee, R.J., C. Karakaya, and H. Zhu, *Process intensification in the catalytic conversion of natural gas to fuels and chemicals.* Proceedings of the Combustion Institute, 2017. **36**(1): p. 51-76.
4. Huang, L., et al., *Optimization of Ni-Based Catalysts for Dry Reforming of Methane via Alloy Design: A Review.* Energy & Fuels, 2022. **36**(10): p. 5102-5151.
5. Sokolov, S., et al., *Stable low-temperature dry reforming of methane over mesoporous La_2O_3-ZrO_2 supported Ni catalyst.* Applied Catalysis B: Environmental, 2012. **113-114**: p. 19-30.
6. Barama, S., et al., *Catalytic properties of Rh, Ni, Pd and Ce supported on Al-pillared montmorillonites in dry reforming of methane.* Catalysis Today, 2009. **141**(3-4): p. 385-392.
7. Ferreira-Aparicio, P., A. Guerrero-Ruiz, and I. Rodríguez-Ramos, *Comparative study at low and medium reaction temperatures of syngas production by methane reforming with carbon dioxide over silica and alumina supported catalysts.* Applied Catalysis A: General, 1998. **170**(1): p. 177-187.
8. Hou, Z., et al., *Production of synthesis gas via methane reforming with CO_2 on noble metals and small amount of noble-(Rh-) promoted Ni catalysts.* International Journal of Hydrogen Energy, 2006. **31**(5): p. 555-561.
9. Ranjekar, A.M. and G.D. Yadav, *Dry reforming of methane for syngas production: A review and assessment of catalyst development and efficacy.* Journal of the Indian Chemical Society, 2021. **98**(1).
10. Velmurugan, S. and P. N, *Recovery of Chemicals from Pressmud – A Sugar Industry Waste.* Journal of Indian Chemical Engineer, 2006. **48**: p. 160-163.
11. Kanaphan, Y., et al., *Interfacially Enhanced Stability and Electrochemical Properties of C/SiOx Nanocomposite Lithium-Ion Battery Anodes.* Advanced Materials Interfaces, 2022. **9**(19): p. 2200303.
12. Deraz, N.M. *The comparative jurisprudence of catalysts preparation methods: I. Precipitation and impregnation methods*. 2017.
13. Ding, F., et al., *Synthesis and Catalytic Performance of Ni/$SiO_2$for Hydrogenation of 2-Methylfuran to 2-Methyltetrahydrofuran.* Journal of Nanomaterials, 2015. **2015**: p. 1-6.
14. Güler, E., et al., *A theoretical study for the band gap energies of the most common silica polymorphs.* Chinese Journal of Physics, 2020. **65**: p. 472-480.
15. Jiang, H., et al., *Photocatalytic Partial Oxidation of Methane on Palladium-Loaded Strontium Tantalate.* Solar RRL, 2019. **3**(7).

16. Takeda, K., et al., *Metal Carbide as A Light-Harvesting and Anticoking Catalysis Support for Dry Reforming of Methane.* Global Challenges, 2019. **4**(1).